EJMO

DOI: 10.14744/ejmo.2023.61011
EJMO 2023;7(1):70–82

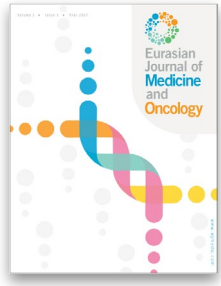

Research Article

Therapeutic Impact of Nano Diosgenin on Metabolic Reprogramming in an Animal Model of Mammary Oncogenesis Modulating Carbohydrate Metabolizing Enzymes

Manobharathi Vengaimaran, Kalaiyarasi Dhamodharan, Mirunalini Sankaran

Department of Biochemistry and Biotechnology, Faculty of Science, Annamalai University, Tamil Nadu, India

Abstract

Objectives: The primary target of this study is to explore a novel therapeutic pathway of nano Diosgenin (DG) by pinpointing the metabolic enzymes that underlies its anti-breast cancer impacts.

Methods: A single dosage of 7.12 Dimethyl Benz(a)anthracene (DMBA) (25 mg/kg b.wt) was injected to induce breast cancer. Oral administration of DG (10 mg/kg b.wt) and DG encapsulated chitosan nanoparticle (DG@CS-NP) (5 mg/kg b.wt) was used to medicate DMBA induced tumor bearing rats just after the emergence of a tumor. After the experimental period, biochemical analyses were carried out.

Results: Mammary carcinoma bearing rats showed a significant rise in the levels of glycolytic enzymes (hexokinase, phosphoglucoisomerase, and aldolase) and the pentose phosphate pathway enzyme (glucose-6-phosphate dehydrogenase). It also elicits a drop in gluconeogenic enzymes (glucose-6-phosphatase and fructose 1, 6- diphosphatase) and mitochondrial enzymes (succinate dehydrogenase and malate dehydrogenase). Contrarily, nano DG dramatically reverted the rates of glycolytic enzymes, pentose phosphate pathway enzymes, gluconeogenic enzymes, and mitochondrial enzymes in the mammary, liver and kidney tissues to near normal tiers on compared to plain DG treated rats. Thereby, confirming its chemotherapeutic prospects on metabolic rewiring.

Conclusion: Thus, our observations suggested that nano DG is a potent therapeutic agent that might have a significant influence on metabolic complications of breast cancer than free DG.

Keywords: 7,12 Dimethyl benz(a)anthracene, cancer cell metabolism, carbohydrate metabolizing enzymes, mammary carcinoma, Nano diosgenin

Cite This Article: *Vengaimaran M, Dhamodharan K, Sankaran M. Therapeutic Impact of Nano Diosgenin on Metabolic Reprogramming in an Animal Model of Mammary Oncogenesis Modulating Carbohydrate Metabolizing Enzymes. EJMO 2023;7(1):70–82.*

Breast cancer is the most prevailing malignant tumor in women and the second capital source of cancer fatalities. It is marked by a stack of genetic mutations and gene deregulations, culminating in unrestrained cell growth that mandates higher energy output and macromolecule biosynthesis.[1,2] In order to handle such an increasing metabolic load, malignant cells often modify their biochemical pathways to expedite instant uptake and breakdown of

Address for correspondence: Mirunalini Sankaran, MD. Department of Biochemistry and Biotechnology, Faculty of Science, Annamalai University, Annamalai Nagar – 608 002, Tamil Nadu, India
Phone: +91 9442424438 **E-mail:** mirunasankar@gmail.com

Submitted Date: August 10, 2022 **Revision Date:** November 26, 2022 **Accepted Date:** December 27, 2022 **Available Online Date:** March 08, 2023

nutrients which promotes disease metamorphosis, maintenance, and progression. Therefore, emerging facts point out that it is not only a genetic disease, but also a metabolic disorder, with oncogenic signaling pathways partaking in energy regulation and anabolism to endorse rapidly spreading tumors.[3] These pioneering insights afforded the template for a contemporary explosion of interest in cancer metabolism studies, which has led revelations of multiple metabolic networks being overactivated and/or reprogrammed in cancer cells.

Metabolic reprogramming is thus seen as a cornerstone of cancer. Noticeably, metabolic reprogramming and its intricate regulatory circuits have an indispensable impact on breast cancer progression and advancement.[4] The Warburg Effect, a pivotal facet of energy metabolism that turns glucose into lactate often in the presence of abundant oxygen, is vital for breast cancer cell growth, longevity, metastasis, and therapeutic resilience. Rising findings states that limiting the Warburg effect were now been proven to be beneficial in suppressing breast cancer proliferation and metastasis. As a consequence, a stronger awareness of the Warburg Effect's regulatory mechanism, primarily the core glycolytic enzymes engaged in aerobic glycolysis, might aid in the invention of glycolysis-based breast cancer therapeutics.[5] Regardless of whether they are in a normoxic or hypoxic milieu, all cancerous cells employ glycolysis as a source of energy. Majority of the cellular glucose reaches the TCA cycle as pyruvate in healthy cells. However, glucose might be consumed for lactate generation or macromolecular synthesis through the pentose phosphate pathway. One molecule of glucose is turned into two molecules of pyruvate in glycolysis, which are principally oxidized to yield acetyl-CoA, which fuels the TCA cycle. Conversely, under hypoxic circumstances, pyruvate can be translated to lactate. Progression through the TCA cycle ensues when elevated energy prerequisites arise. Gluconeogenesis, a process that is reciprocally controlled with glycolysis in order to retain the cell's metabolism optimal, may also produce glucose. Originally, it was hypothesized that these metabolic alterations were due to disruption in mitochondrial oxidative phosphorylation, signifying that cancer cells were struggling to respire efficaciously to get adequate ATP.[6, 7] Moreover, in intact glycolytic cancer cells, only 10% of the pyruvate reaches a curtailed Krebs cycle. The dysregulation of action of the Krebs cycle enzymes promotes a drop in cumulative net ATP synthesis in the presenter cells which contributes to a depletion of body weight and, as a response, cancer cachexia arises.

At present, applicable breast cancer therapeutic approaches still remain as a palliative care and none of them relies under curative care. As current conventional modalities such as surgery, radiation therapy, hormonal therapy, and immunotherapy have proven ineffective, resulted in a clinical deficit owing to drastic health consequences and multidrug resistance. One of the prime peculiarities of cancer therapeutic interventions is the potential to acquire remit, which is almost invariably accompanied by resurgence.[8] Therefore, nutritional therapy seems to be an integral aspect of cancer cachexia therapeutics and it can even assist to limit the progress of cancer in certain instances. According to an accumulating amount of evidence, a multitude of micronutrients exhibit anti-cancer qualities.[9] Recently, countless cancer researchers are focused on the naturally procured dietary steroidal saponins as a curative target for multiple cancers. As several reports exist on its *in vitro* and *in vivo* cytotoxicity domain, steroidal saponins have been posed as a proven promising therapeutic candidate for a variety of cancers.[10] Among various food saponins, Diosgenin (DG) (3β,25R)-spirost-5-en-3-ol, a potent steroidal sapogenin seems to be explicitly employed as a core ingredient in countless traditional and patented Chinese medicines owing to its epic multi-layered therapeutic treasures. It was primarily spotted on *Dioscorea species*, *Heterosmilax* species, and *Trigonella foenum-graecum*. It is also abundantly visible in the tubers of diverse wild yams (*Dioscorea* villosa Linn). Although, it was detected in 137 distinct *Dioscorea* spp., 41 of them will have upwards of 1% DG matter. Fenugreek seeds (*Trigonella foenum graecum* Linn) and *Dioscorea zingiberensis* rhizomes are also strong suppliers of DG. Besides that, *Trillium govanianum* and *Costus speciosus* comprise nearly 2.5% and much more than 2.12% DG content, respectively.[11] Thereby, promises to be a fruitful bioactive chief compound of interest for breast cancer prevention and therapy at both biochemical and molecular levels with zero level of toxicity.[12] Although it has an expansive chemotherapeutic repertoire in treating divergent cancers, its pharmaceutical formulation has been hampered by its poor aqueous solubility (0.02 mg/L), inadequate bioavailability and pharmacokinetics, and rapid biotransformation under several physiological conditions.[13] To enhance its therapeutic profile, we formulate DG nanoparticles using CS as an encapsulated carrier which culminates in an improved bioavailability, strong drug payload, and controlled drug delivery at the target site. Therefore, with this background, we designed the current study to unravel the therapeutic impact of nano DG on metabolic reprogramming in an animal model of mammary oncogenesis through modulating carbohydrate metabolizing enzymes.

Methods

Chemicals

DG, Chitosan, 7,12 Dimethyl benz(a)anthracene (DMBA), and sodium tripolyphosphate (TPP) were purchased from Sigma-Aldrich Co. Ltd. All additional chemicals including solvents used were of high purity and of analytical grade marketed by HiMedia, Sisco Research Laboratories Pvt. Ltd., Mumbai, India, and from local commercial outlets.

Preparation of DG@CS-NP

DG encapsulated Chitosan nanoparticle (DG@CS-NP) was fabricated using Ionic gelation method which is based on electrostatic interactions between cationic CS and anionic TPP as a cross-linker.[14] CS-NP synthesis procedure has been optimized at different concentration levels and dissolved in 1% (v/v) of glacial acetic acid. The solution was stirred continuously for overnight at room temperature and the solution pH was balanced to 5.0 using 1 M NaOH. DG at three different concentrations (25, 50, and 100 mg) (dissolved at 0.5 % (v/v) of DMSO) was then added to the freshly made CS dispersion and stirred for 1 h. After that, an equal amount of TPP (1 mg/ml) was added to the CS-DG solution with a mild stirring effect. The resultant mixture solution has been allowed to stir for 1 h to form DG@CS-NP. The entire procedure was performed under room temperature. Prepared nanoparticles have been separated by centrifugation. The pellets were collected and dried and stored in a refrigerator at 4°C for future evaluation. These lyophilized samples were further characterized by UV-visible spectroscopy, Encapsulation efficiency (EE), drug loading capacity, FTIR assessments, *in vitro* drug release study, X-ray diffraction analysis (XRD), and also by thermogravimetric analysis (TGA).

Characterization of DG@CS-NP

UV-Visible Spectroscopy

UV-visible spectra were collected from the UV-visible spectrophotometer, Shimadzu UV-1800 model, Japan. All spectra were recorded by measuring between 200 and 800 nm and corrected against CS as background.

Diosgenin Loading Efficiency

The proportion of DG suffocated in the nanocomposites system has been quantified obliquely by calculating the ratio of DG residing in the supernatant on the basis of sample absorption at 250 nm. The standard curve was obtained and the absorbance of the sample was gauged in 3 mL quartz cuvettes utilizing Shimadzu UV-1800. Assessment besides validating the amount of drug stuffed into nanomaterials is the entrapping efficacy of drug (EE). The determination of the EE allows for the optimization of the amount added, the reduction of the waste and is defined as follows:

$EE = [Drug_{Total} - Drug_{Free} / Drug_{Total}] \times 100$

$Loading\ Capacity = [Drug_{Total} - Drug_{Free} / Weight\ of\ nanoparticle] \times 100$

Entrapment efficiency is an interpretation of the quantity of the drug trapped inside the nanocomposite as it relates to the initial drug loading it. 100% EE means that the whole quantity of the drug added has been integrated into the nanoparticle.

FT-IR Analysis

The FT-IR sample spectra were measured using a Perkin-Elmer, FT-IR spectrophotometer, USA, within a range of 4000–400 cm^{-1}. FTIR is used to validate a cross-linking interaction between both the TPP phosphoric group and the DG@CS amino group. The pellets have been formulated by homogeneously dried composition in dried KBr in a mortar and pestle, and then the powder was compacted under vacuum using a round, flat-sided smash to deliver compressed pellets. Approximately, 5 mg of the sample was mixed with 100 mg KBr and compacted into a pellet using such hydraulic press. All spectra were corrected against the KBr pellet reference spectrum.

In Vitro Drug Release

In vitro drug release study was performed in the PBS medium according to Dudhani and Kosaraju.[15] DG@CS-NP 10 mg/ml was resuspended in a dialysis membrane bag with a molecular cut off of 10 kDa. The membrane bag has been placed in 20 ml of PBS (pH 7.4) under magnetic stirring at 120 rpm, temperatures maintained at 37°C. The amount of DG that was released from the dialysis bag was calculated at various time intervals (5, 10, 15, 20, 25, 35, 45, 55, 65, and 75 h) by measuring the absorbance values at 390 nm. A calibration curve was plotted with the concentration against the absorbance values. Results collected from the *in vitro* drug release for formulation in different release media have been adapted to different kinetic models. Each evaluation was done in a triplicate and the release of DG has been calculated from the following equation:

Release rate (%) = [Released DG/Total DG] × 100

XRD Analysis

The metallic nature of the resultant nanoparticles was probed using the XRD technique. The synthesized DG@CS-NP was centrifuged for 5 min at 8000 rpm. The resultant plate was then centrifuged 3 times after being dissolved in 10 mL of sterile deionized water, and it was dried for 24 h in a vacuum oven. The generated nanoparticle's structure and

content were finally examined using XRD (Philips Xpert Pro, The Netherlands, Amsterdam).[16]

TGA Analysis

A Perkin-Elmer Model of TGA-7 thermogravimetric system with a microprocessor driven temperature control unit and a TA data station was used. The mass of the samples was generally in the range of 2–3 mg. The sample pan was placed in the balance system equipment and the temperature was raised from 25 to 800°C at a heating rate of 10°C per minute with the nitrogen flow rate of 50 cm^3/min. The mass of the sample pan was continuously recorded as a function of temperature.

Animal Model

Six to eight weeks old adult female Sprague Dawley rats weighing 130–150 g was purchased from Biogen Laboratory Animal Facility, Bangalore, India. Animals were housed in six spacious polypropylene cages under typical laboratory norms: temperature (27±2°C) and humidity (55±5%) with a 12 h light/dark cycle and standard food and water provided in the Central animal house, Rajah Muthiah Medical College, and Hospital, Annamalai University. The rats were allowed a week to acclimatize before the trial began. The experimental approach was officially validated by Annamalai University's Institutional Animal Ethics Committee (IAEC) directed by the Committee for the Purpose of Control and Supervision of Experimental Animals (CPCSEA) (Registration number 160/PO/ReBi/S/1999/CPCSEA). (Proposal No. 1241 dated April 23, 2019). The animals were maintained by in accordance with the Indian National Law on Animal Care and Use, as well as the Annamalai University's ethical committee for animal experimentation's specifications and suggestions.

Tumour Induction

Female Sprague Dawley rats were administered with DMBA (25 mg/kg body weight), a dose intended to make sufficient tumor incidence in the control group over the course of the study. The DMBA was dissolved in a 1 mL emulsion of sunflower oil (0.75 mL) and physiological saline (0.25 mL).[17]

Experimental Design

The animals were sorted into six groups, each with six animals, and were assigned randomly to the experimental and control groups. As a control, animals from Group I were used. Groups II-V were administered a single subcutaneous injection of 25 mg/kg b.wt DMBA during the 1st week of the trial. After 7 weeks, Groups III and IV were received DG and DG@CS-NP 3 times a week (using oral gavage tube), at 10 mg/kg b.wt and 5 mg/kg b.wt (1 mL) separately. Groups V and VI rats were administered CS-NP and free DG@NP orally 3 times a week (21 days) at a dose of 5 mg/kg b.wt. The dosage used in this analysis is premised on the previous literature.[18, 19] The experiment was terminated after 14 weeks, and all rats were sacrificed by administering ketamine at a dose of 60 mg/kg body weight. Blood was collected in heparinized tubes and centrifuged at 1000× g for 15 min to separate serum and plasma. The biochemical analysis was conducted using such samples. The liver and kidney tissue were quickly dissected, washed thoroughly using ice-cold saline. Then a part of the tissue was homogenized in 0.1M Tris hydrochloric acetic acid buffer (pH=7.4) before being centrifuged at 3000g for 10 min at 40°C. The supernatant was collected and processed to assess specific biochemical parameters.

Biochemical Analysis

Assessment on Carbohydrate Metabolizing Enzymes

Hexokinase (HK) activity was assessed in terms of the amount of glucose used after the addition of ATP.[20] The activity of aldolase was measured using the King (1965) [21] technique, which used fructose^{-1}, 6-diphosphatase (F1,6-DP) as a substrate and dinitrophenyl hydrazine as a coloring reagent. According to Gracy and Tilley's (1975)[22] approach, phosphoglucoisomerase (PGI) was tested using 2, 6-dichlorophenol indophenols dye. The activity of glucose-6-phosphate dehydrogenase (G-6PD) was quantified in terms of the quantity of inorganic phosphorus released after the addition of the substrate glucose-6-phosphate (G-6P) using the Ells and Kirkman (1961)[23] technique. The activity of G-6P and F1,6-DP was measured[24] in aspects of the quantity of inorganic phosphorus liberated when their respective substrates, G-6P and, F1,6-DP were added. The integrity of mitochondria was evaluated by quantifying succinate dehydrogenase (SDH) activity using the Slater and Bonner (1952)[25] technique, which estimates the rate of potassium ferricyanide reduction. The activity of malate dehydrogenase (MDH) was determined using the Mehler et al. (1948)[26] approach.

Estimation of Hexokinase

The incubation mixture contains 2.5 mL of buffer, 1.0 mL of substrate, 0.5 mL of ATP, 0.1 mL of each of MgC12, NaF, 0.4 mL each of dipotassium hydrogen phosphate and potassium chloride and 2.5 mL of Tris-HCI buffer (pH 8.0). The mixture was pre-incubated at 37°C for 5 min. The reaction was initiated by the addition of 2.0 mL of tissue homogenate. 1.0 mL aliquot of the reaction mixture was removed immediately into tubes containing 1.0 mL of 10% TCA. A second aliquot was removed after 30 min of incubation at 37°C. The precipitated protein was removed by centrifuga-

tion and the residual glucose in the supernatant was estimated. A reagent blank was run with each test. The difference between the two values gave the amount of glucose phosphorylated.

Estimation of Phosphoglucoisomerase

1.0 mL of buffered substrate and 0.1 mL of enzyme was incubated at 37°C for 30 min. The reaction was arrested by adding 1.0 mL of 10% TCA and centrifuged. To 1.0 mL of the supernatant, 9.0 mL of color reagent was added and heated in water bath at 70°C for 15 min. The standard was also treated similarly. The tubes were cooled in running water and the color developed was read at 420 nm using a spectrophotometer.

Estimation of Aldolase

The incubation mixture containing 1.0 mL of buffer, 0.25 mL of substrate, 0.25 mL of hydrazine sulfate, and 0.1 mL of enzyme. This was incubated at 37°C for 15 min. The reaction was terminated by adding 1.0 mL of 10% TCA and the tubes were centrifuged. To the aliquot of supernatant, 1.0 mL of 0.75 N NaOH was added and left at room temperature for 10 min. The color developed after the addition of 1.0 ml of 0.75 N NaOH was read at 540 nm using spectrophotometer. The enzyme activity was expressed as n moles of glyceraldehyde formed/mg protein/min.

Estimation of Glucose-6-Phosphate Dehydrogenase

To 0.4 mL of tris-HCl buffer, 0.2 mL of NADP, 0.2 mL of magnesium chloride, 1.0 mL of water and 0.2 mL of enzyme were added in a cuvette. The reaction was started by the addition of 0.2 mL of G-6P and the increase in optical density was measured at 340 nm.

Estimation of Glucose-6-Phosphatase

The incubation mixture in a total volume of 1.0 mL contained 0.3 mL of buffer, 0.5 mL of substrate and 0.2 mL of enzyme extract. The incubation was carried out at 37°C for 60 min. The reaction was terminated by the addition of 1.0 mL of 10% TCA and centrifuged at 2500 rpm for 15 min. The suspension was centrifuged and the inorganic phosphate content of the supernatant was estimated.

Estimation of Fructose-1,6-diphosphatase

The assay mixture in a total volume of 2.0 mL contained 1.5 mL buffer, 0.1 mL substrate, 0.25 mL MgCl2, 0.1 mL KCl, 0.25 mL EDTA, and 0.1 mL enzyme. This mixture was incubated at 37°C for 15 min. The reaction was terminated by the addition of 1.0 mL TCA. The suspension was centrifuged and the inorganic phosphate content of the supernatant was estimated.

Estimation of Succinate Dehydrogenase

Added 0.75 mL of phosphate buffer, 0.1 mL of KCN, 0.2 mL sodium succinate, 1.3 mL water, 0.1 mL DCPIP, and 0.5 mL PMS. The reaction was started by the addition of 0.2 mL of mitochondrial fraction and the change in absorbance at 600 nm during the first 3 min at 30 s interval was noted. A blank rate (all reagents except succinate) must be determined separately.

Estimation of Malate dehydrogenase

The reaction mixture contains 0.3 mL of phosphate buffer, 0.1 mL of NADH, 0.1 mL of oxaloacetate and 2.4 mL of water. The reaction was carried at 25°C and was started by the addition of 0.1 mL of mitochondrial suspension. The control tubes contained all reagents except NADH. The change in OD at 340 nm was measured during the first 2 min at 15 s intervals.

Statistical Analysis

A statistical analysis was performed using SPSS V26.0 (IBM SPSS, USA) software package. The data were expressed as mean ± standard deviation (SD). One-way analysis of variance (ANOVA) followed by Tukey's post hoc test was used to correlate the difference between the variables. A value of $p<0.05$ was considered statistically significant.

Results

Characterization of synthesized DG@CS-NP

UV- Visible Spectroscopic Analysis

The UV-Visible spectrum of DG encapsulated CS-NP at three different concentrations (25, 50, 100mg) are shown in Figure 1. The Plasmon absorption peak appeared at 280

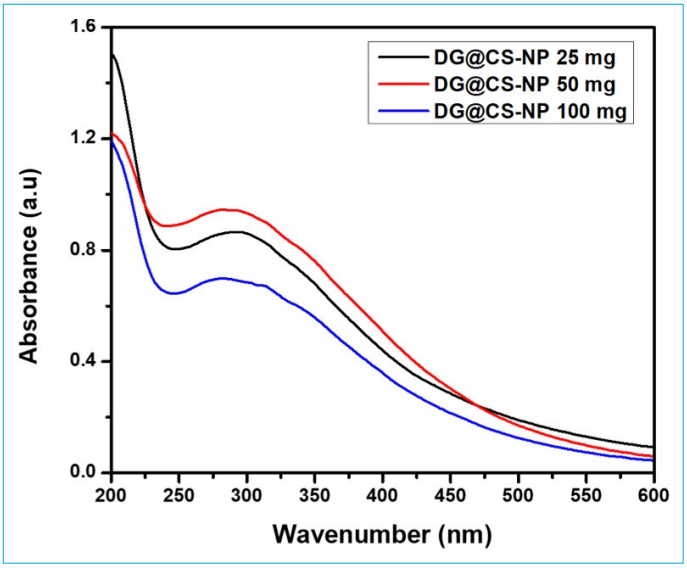

Figure 1. UV-visible spectrum of DG@CS-NP (25, 50, 100mg).

nm, stating the formation of DG nanoparticles. It is evident from the UV-Visible spectral studies that the size of the nanoparticles ranged up to 20 nm.

Encapsulation Efficiency & Loading Capacity of DG@CS-NP

Continuing to the DG@CS-NP synthesis, encapsulation and loading Efficiency was computed on the basis of spectral absorption of UV findings. As shown in Table 1, the optimal loading and encapsulation concentration were observed by fluctuating the DG volume in the CS/TPP ratio (4:1). The drug concentration of 100 mg DG displays an elevated encapsulation and loading throughput of 95.29±1.30% and 36.56±1.85%. Other concentrations were noted to have lessened loading and drug encapsulation efficacy as shown in Table 1.

FT-IR Spectrum of DG@CS-NP:

The FTIR spectra of DG@CS-NP (25, 50, and 100 mg) are shown in Figure 2. This demonstrates a functional group such as -OH stretching at 3257 cm^{-1} related to alcoholic/phenolic groups, -C-O ether group throttle vibrations at 1032 cm^{-1}, C=O torque vibration ester group at 1674 cm^{-1}, and C-H Stretching alkane vibration at 2863 cm^{-1}, respectively, to DG. The observed peak of CS was assigned to the N-H range of 3463 cm^{-1} and the transition to the interior at the same spectral peak (3374 cm^{-1}) of the DG@CS-NP confirms the formation of DG with CS. The N-H bending vibration and the C-O stretching of the alcohol group were assigned to 1674 cm^{-1}. C-N, N-H, and C-H stretching vibrations were delegated to the 1324 cm^{-1}, 1510 cm^{-1}, and 2870 cm^{-1} bands, respectively. The key characteristic absorption spectrum of CS appeared at 1495 cm^{-1}. The resulting complex also showed a lack of C=S (1202 cm^{-1}) and C-N (1373 cm^{-1}). DG related spectral peaks in DG@CS nanoparticles, likely due to the interaction between DG and CS. The decline in the intensity of stretching and the lack of a spectral peak could be due to the massive interference of the functional group in the configuration of bonds, implying with no structural reforms in the DG@CS-NP.

In-Vitro Drug Release Profile of DG@CS-NP:

The primary motive for pursuing nanocomposites is just to deliver the drugs in a controlled and sustained manner. For

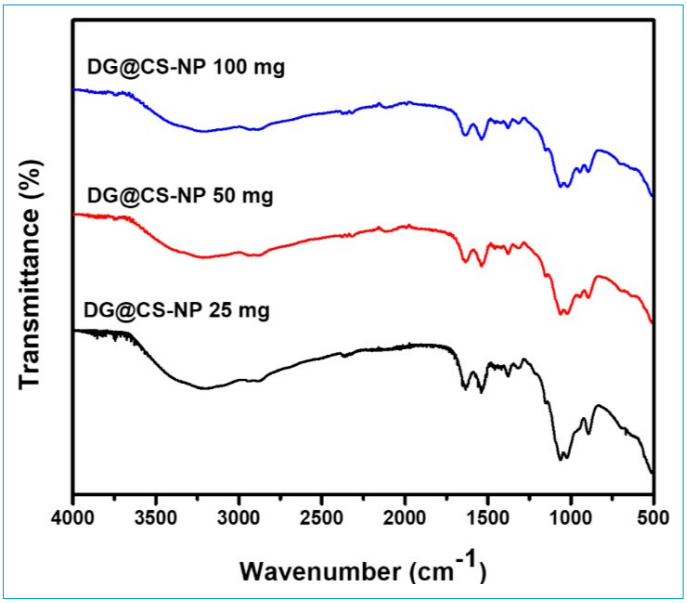

Figure 2. FT-IR spectral analysis of DG@CS-NP (25, 50, 100 mg).

that, recognizing the way and the duration at which they released the drug is more important in drug delivery. To achieve these information's, the releasing method must allow the drug and the carrier vehicle to segregate separately. [27] Drug release studies are often used to quantify the duration of the sustained drug release from its carrier. The *in vitro* drug release of DG from DG@CS-NP at different time intervals was investigated at three different concentrations (25, 50, and 100 mg) and their resulting data are shown in Figure 3. This study was implemented in a pH 7.4 phosphate buffer at 37°C. Due to the hydrophobic nature of DG, it was encapsulated with CS-NP. Typically, hydrophobic substances have a sluggish release rate leading to decreased diffusion. Conversely, hydrophilic drugs such as cationic polymer CS display rapid release due to its elevated soluble in water. DG expressed sustained release tendencies with a constant growth in cumulative release of drugs up to 75 h. This shows a sustainable release of the drug in the composition. It was notable that the preparation exhibited an initial release of the rupture probably due to the small size of the NPs.

XRD Analysis

Figure 4 displays the XRD patterns of CS and DG@CS-NP (100 mg) in their respective forms. The typical peaks of

Table 1. Encapsulation efficiency & drug loading capacity of DG@CS-NP

Concentration of CS-DG (mg)	Concentration of DG (mg)	Encapsulation efficiency (wt %)	Drug Loading (wt %)
CS- DG-25%	25	79.71±1.28	19.24±1.06
CS- DG -50%	50	91.35±1.09	32.93±1.32
CS- DG-100%	100	95.29±1.30	36.56±1.85

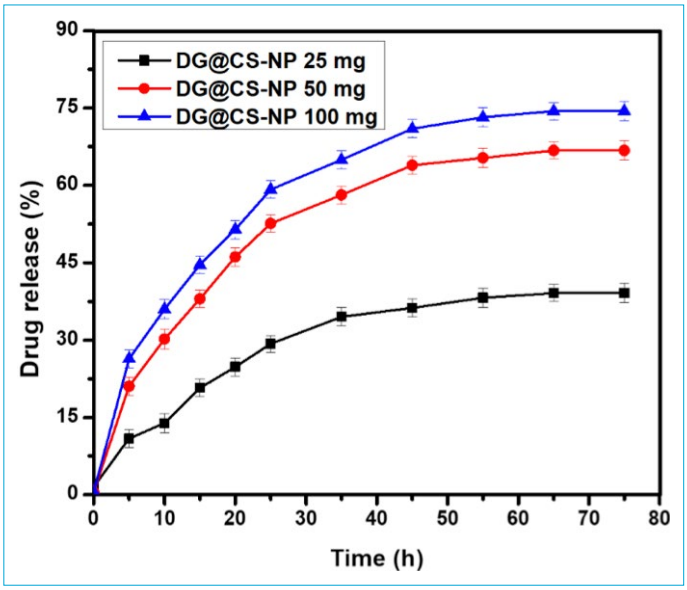

Figure 3. In-vitro drug release profile of DG@CS-NP (25, 50, 100mg).

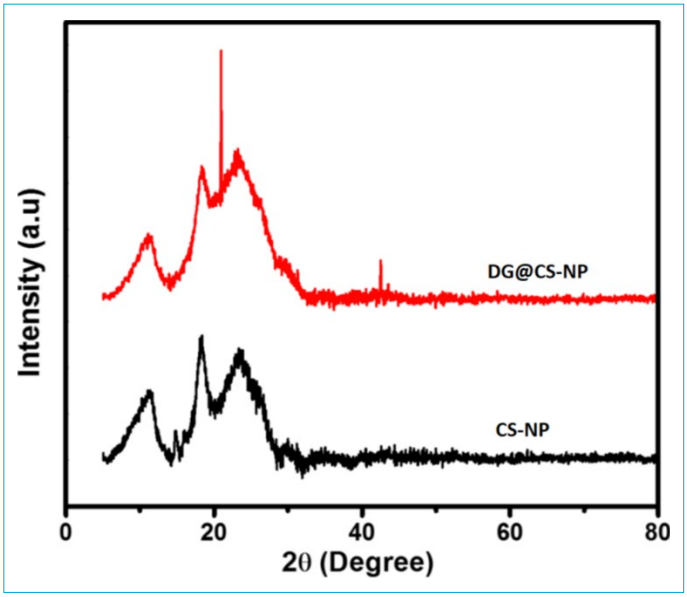

Figure 4. X-ray diffraction analysis of CS and DG@CS-NP (100mg).

CS nanoparticles were seen at angles of 12°, 18°, and 25°, respectively. Similar peaks were seen in DG@CS-NP, although the strength was less than what was seen in pure CS nanoparticles. This might be because the DG was incorporated into the CS nanoparticles.

TGA Analysis

TGA was used to study the thermal decomposition of CS and DG@CS-NP (100 mg), and the findings are shown in the Figure 5 They displayed a four-step degradation pattern. CS-NP initially lost 10% of its weight when heated to 140°C. The second step decomposition of polymer (CS) in the graph illustrates with a weight loss of about 12% at 202°C. DG@CS-NP started its degradation at 206°C, where-

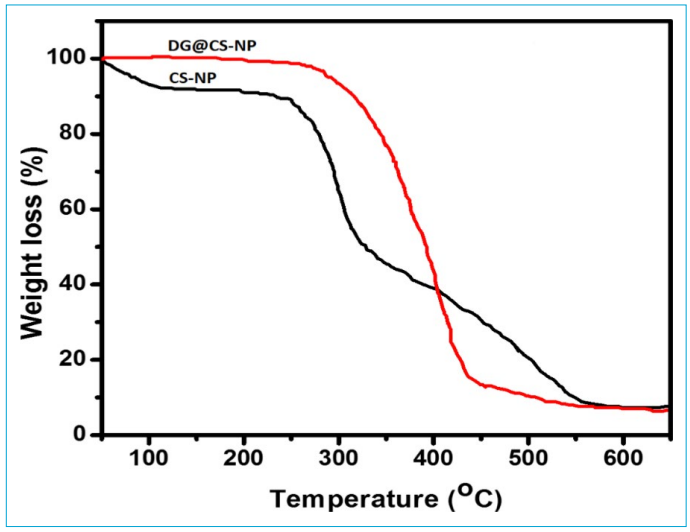

Figure 5. Thermogravimetric analysis of CS and DG@CS-NP (100mg).

as the melting point is within this range of temperatures. At 303°C, the third phase was seen with a weight loss of 7% for DG@CS-NP and 50% for CS. However, at 550°C, weight loss of almost 90% has been observed in both CS and DG@CS-NP during the fourth stage of decomposition.

Biochemical Analysis

Impact of DG@CS-NP on Carbohydrate Metabolizing Enzymes

The effect of DG@CS-NP on the levels of HK, PGI and aldolase activity on mammary, liver and kidney tissues of both control and experimental rats were presented in Figures 6-8. The contents in DMBA-administered rats (Group II)

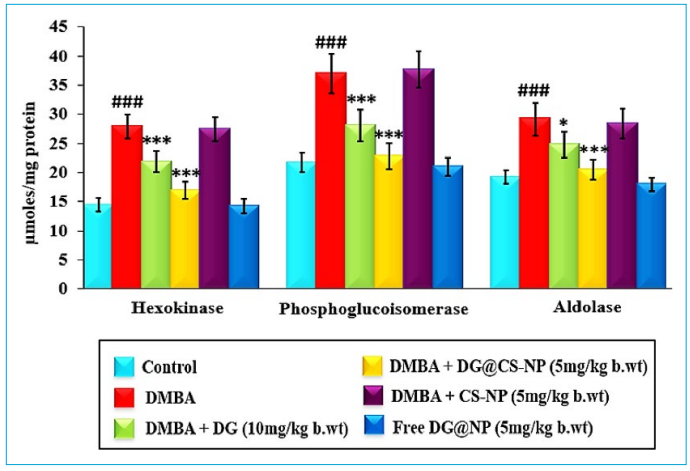

Figure 6. Impact of DG@CS-NP on the quantities of glycolytic markers (hexokinase, phosphoglucoisomerase and aldolase) in the mammary tissue of control and experimental rats.

*Values are expressed as mean±SD for six rats in each group. Significant levels are ###p<0.001 when compared with control group and *p<0.05, ***p<0.001 when compared with DMBA group.*

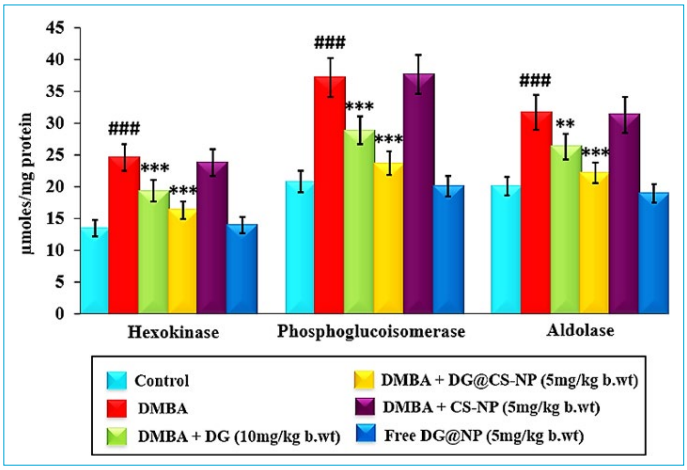

Figure 7. Impact of DG@CS-NP on the quantities of glycolytic markers (hexokinase, phosphoglucoisomerase and aldolase) in the liver tissue of control and experimental rats.

*Values are expressed as mean±SD for six rats in each group. Significant levels are ###p<0.001 when compared with control group and **p<0.01, ***p<0.001 when compared with DMBA group.*

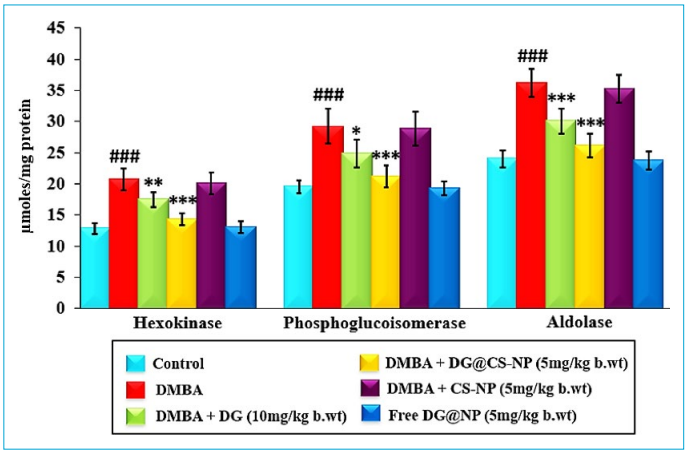

Figure 8. Impact of DG@CS-NP on the quantities of glycolytic markers (hexokinase, phosphoglucoisomerase and aldolase) in the kidney tissue of control and experimental rats.

*Values are expressed as mean±SD for six rats in each group. Significant levels are ###p<0.001 when compared with control group and *p<0.05, **p<0.01, ***p<0.001 when compared with DMBA group.*

were notably higher than in control rats (Group I). In contrast to DMBA-induced (Group II) rats HK, PGI and aldolase quantities, oral dosing of DG 10mg/kg b.wt (Group III) and DG@CS-NP 5mg/kg b.wt (Group IV) resulted in drastically reduced tiers of HK, PGI and aldolase. There have been no substantial changes between rats treated with free DG@NP (Group VI) alone and control rats (Group I). Moreover, it was proved that DG@CS-NP 5 mg/kg b.wt was much more active than DG 10 mg/kg b.wt in influencing the levels of glycolytic enzymes.

Figure 9 reveals the proportions of G-6PD enzymic activity on the mammary, liver and kidney tissues of both the control and experimental rats. The levels are much considerably higher in DMBA-administered rats (Group II) than those in control rats (Group I). Oral treatment of DG 10mg/kg b.wt (Group III) and DG@CS-NP 5 mg/kg b.wt (Group IV) indicates dramatically reduced G-6PD levels in comparison with DMBA-induced (Group II). Conversely, CS-NP 5mg/kg b.wt (Group V) orally medicated rats exhibit no significant changes when compared to DMBA-induced rats (Group II). There were no significant differences amongst free DG@NP (Group VI) alone treated rats and control rats (Group I). Ultimately, DG@CS-NP 5mg/kg b.wt was evidenced to be more effective in modulating G-6PD levels than DG 10mg/kg b.wt.

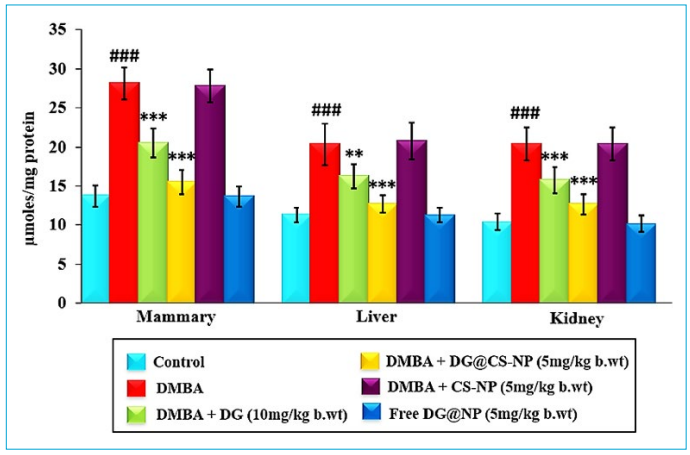

Figure 9. Impact of DG@CS-NP on the quantities of glucose 6-phosphate dehydrogenase enzyme in the mammary, liver and kidney tissue of control and experimental rats.

*Values are expressed as mean±SD for six rats in each group. Significant levels are ###p<0.001 when compared with control group and **p<0.01, ***p<0.001 when compared with DMBA group.*

Figures 10 and 11 indicate the levels of gluconeogenetic enzymes (G6-P and F1,6-DP) on mammary, liver and kidney tissues of both control and experimental group animals. G6-P and F1,6-DP levels significantly lower in DMBA-induced rats (Group II) when compared with control rats (Group I). Fortunately, oral administration of DG 10 mg/kg b.wt (Group III) and DG@CS-NP 5mg/kg b.wt (Group IV) depicts significantly escalated levels of G6- P and F1,6-DP on compared with DMBA rats (Group II). When CS-NP 5mg/kg b.wt (Group V) treated rats were compared to DMBA group rats (Group II), no variations were noted. Despite this, no significant differences were recorded in free DG@NP (Group VI) alone treated rats when compared to control rats (Group I). In terms of gluconeogenetic enzymatic levels, DG@CS-NP 5 mg/kg b.wt was reported to be quite effective than DG 10 mg/kg b.wt.

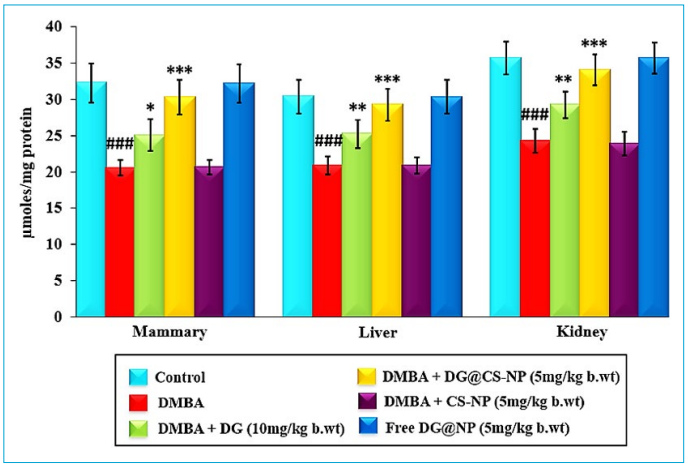

Figure 10. Impact of DG@CS-NP on the quantities of Glucose 6-phosphatase enzyme in the mammary, liver and kidney tissue of control and experimental rats.

*Values are expressed as mean±SD for six rats in each group. Significant levels are ###p<0.001 when compared with control group and*p<0.05, **p<0.01, ***p<0.001 when compared with DMBA group.*

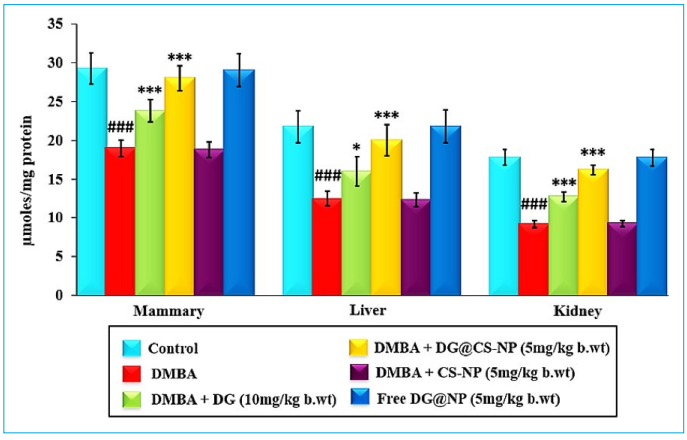

Figure 11. Impact of DG@CS-NP on the quantities of Fructose 1,6-di-phosphatase enzyme in the mammary, liver and kidney tissue of control and experimental rats.

*Values are expressed as mean±SD for six rats in each group. Significant levels are ###p<0.001 when compared with control group and *p<0.05, ***p<0.001 when compared with DMBA group.*

Figures. 12 and 13 portray the concentrations of mitochondrial TCA cycle enzymes (SDH and MDH) on mammary, liver and kidney tissues of both the control and experimental rats. The concentrations of mitochondrial enzymes significantly diminished in DMBA induced cancer bearing rats (Group II) when compared with the control group rats (Group I). Contrasted with DMBA (Group II) rats, oral administration of DG 10 mg/kg b.wt (Group III) and DG@CS-NP 5 mg/kg b.wt (Group IV) exhibit significantly escalated mitochondrial enzymatic levels. While CS-NP 5 mg/kg b.wt

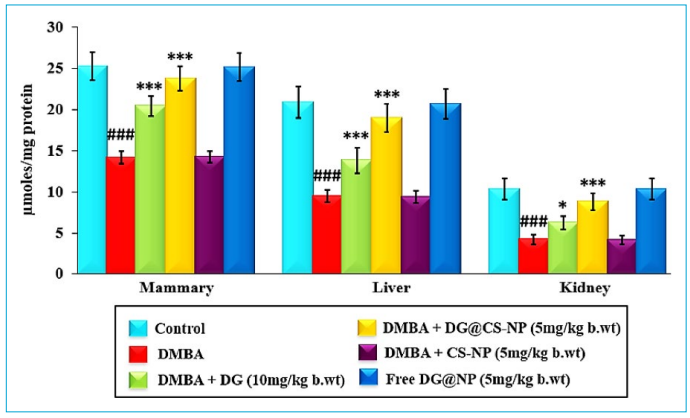

Figure 12. Impact of DG@CS-NP on the quantities of succinate dehydrogenase enzyme in the mammary, liver and kidney tissue of control and experimental rats.

*Values are expressed as mean±SD for six rats in each group. Significant levels are ###p<0.001 when compared with control group and *p<0.05, ***p<0.001 when compared with DMBA group.*

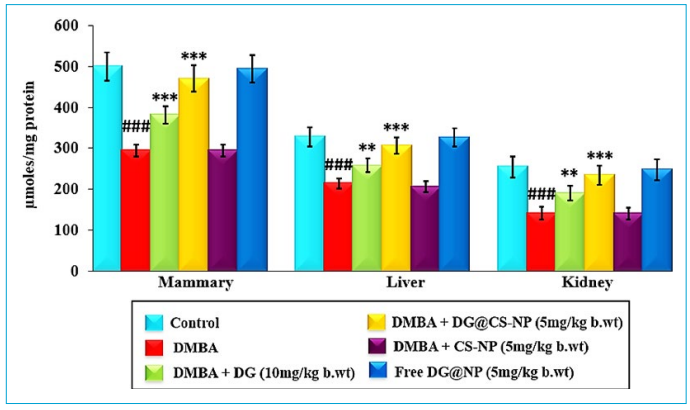

Figure 13. Impact of DG@CS-NP on the quantities of malate dehydrogenase enzyme in the mammary, liver and kidney tissue of control and experimental rats.

*Values are expressed as mean±SD for six rats in each group. Significant levels are ###p<0.001 when compared with control group and*p<0.05, **p<0.01, ***p<0.001 when compared with DMBA group.*

(Group V) treated rats were compared to DMBA (Group II) rats, no modifications were identified. Conversely, Free DG@NP (Group VI) alone administered rats indicates no significant differences in the amounts of mitochondrial enzymes when compared to control rats (Group I). It was unearthed that DG@CS-NP 5 mg/kg b.wt was more robust than DG 10 mg/kg b.wt on regulating mitochondrial TCA cycle enzymes

Discussion

Metabolism is an energy-producing operation in which cells benefit from it for sustaining cellular equilibrium, as

well as for growth and proliferation. The modification of intracellular signaling cascades impaired by aberrant oncogenes and tumor-suppressor genes is a primary significant consequence of cancer cell metabolism.[28] Cancer cells' metabolic priorities diverge drastically from that of healthy cells, offering up a novel therapeutic aperture. In mammary cancerous cells, metabolic reprogramming boosts their growth, survivability, amplification, and sustenance.[29] At present, numerous medications that address cancer metabolism are in clinical trials due to cancer cells metabolic susceptibility. Medications like chemotherapeutic agent, that target cancer cell metabolism utterly having negative impacts that impair a patient's health and quality of life. Contrarily, pharmaceuticals derived from nature womb have lower toxicity and negative effects. Quite a few phytochemicals have indeed been noticed to influence cancer metabolism till date. As a response, increased natural components must be explored for their inhibitory influence on cancer's expanding hallmarks, including metabolism.[30] DG, a naturally procured steroidal saponin, has been extensively explored as a cancer blocker; although, its impacts on cancer metabolism were still unclear. As an outcome, we uncover a novel aspect of DG's anticancer mechanisms in this study. Unfortunately, there seem to be notable downsides coupled with DG's solubility and bioavailability, which constrain its use in clinical contexts. Therefore, in order improve its physicochemical characteristics we fabricate nano DG encapsulated into CS, a biodegradable carrier. CS acts as a vehicle and drop its passenger DG into its target area. This strengthens the notion that nano DG explore its complete onco-pharmacological impacts.[31]

Carbohydrate metabolism is one of the most prominent and profound in carcinogenic tissues, primarily those with increased proliferation patterns and the ability to use and catabolize glucose at excessive rates. More than a century ago, Otto Warburg originally reported that elevated glucose consumption and relying on glycolysis rather than oxidative phosphorylation were the major metabolic hallmarks of cancerous cells. Accelerated glycolysis promotes cancer cell survival and is tied to carcinogenic transition. Current research has revealed that hypoxic tumors preferentially use glucose for glycolytic energy generation, whereas oxygenated tumor cells emit lactic acid, which feeds oxidative metabolism.[32] For aggressively expanding tumors, a rapid glycolysis rate is significant not only as a principal metabolic generator, but also as an origin of precursors for nucleotide and lipid biosynthesis. Although abnormalities of glycolytic and gluconeogenic routes are universally recognized through biochemical explorations of cancer situations, the early alterations in carbohydrate metabolism seem to be of peculiar concern.[33] Glycolysis blockage or retardation has been reported to be efficacious in limiting the progression of cancer, highlighting that glycolysis is vital for cancer proliferation, infiltration, and metastasis. Glycolysis can be halted by blocking the vital glycolytic enzymes which drives the irrevocable events. HK, a prime metabolic enzyme actively engaged in the onset and maintenance of significant glucose catabolic ratios in quickly emerging cancers, and it phosphorylates glucose to G-6P to permit glucose to engage into glycolytic cascade. The energy demands of actively multiplying cells are addressed by ATP released via glycolysis, which is switched from oxidative to glycolytic metabolism in proliferating cells.[34] PGI, a second glycolytic enzyme that catalyses the isomerization of G-6P into F-6P. As a result, PGI is a strong indicator of tumor progression and is raised greatly in malignant cells. Another critical enzyme in the glycolytic pathway, aldolase, was upregulated in tumors. It was discovered to be higher in tumor bearing animals and breast cancer sufferers. PGI and aldolase activity may be enhanced due to cell damage and death. Carcinogen-induced damage is exacerbated in cells in experimental carcinogenesis, and glycolysis is typically noted following a period of tremendous oxygen absorption.[35] Admittedly, our report also proves that the levels of the key glycolytic enzymes (HK, PGI, and aldolase) in mammary, liver, and kidney tissues of DMBA-induced rats displayed relatively high. Whereas, DG and DG@CS-NP treatment substantially suppressed enzymatic levels. Comparatively, DG@CS-NP poses an appreciable therapeutic potency than DG in regulating glycolysis.

The pentose phosphate pathway (also termed as the hexose monophosphate shunt) is where the oxidative glycolysis originates when glucose catabolism is redirected. It is a pivotal metabolic circuit that operates parallel to glycolysis. Thereby, it produces NADPH and ribose-5-phosphate, a molecule that serves as a precursor for the biosynthesis of nucleotides. There are two phases: The first one is oxidative, in which NADPH is produced, and the next is non-oxidative, in which 5 carbon sugars are produced. It also supplies NADPH for fatty acid biosynthesis and cellular longevity in challenging scenarios featuring elevated amounts of intracellular reactive oxygen species. Although disrupting the hexose monophosphate shunt channel correlates directly to cell proliferation and survival, there is mounting evidence that cancerous cells modify the fluxes for their own advantages.[36] G-6PD in the HMP is a prime enzyme which turns G-6P to 6-phosphogluconate. G-6PD deficit has been tied to a diminished chance of cancer that probably due to a drop of mutagenic oxygen-free radicals and nicotinamide-adenine dinucleotide-phosphate for proliferating cells.[37] In our results, contrast to DMBA-administered rats, DG and DG@CS-NP dosage effectively diminished levels of

G-6PD. DG@CS-NP has been reported to be highly active than DG at influencing the levels of G-6PD enzymes.

Gluconeogenesis is the reverse pathway of glycolysis that uses lactate or amino acids to fuel biosynthetic pathways. F^{-1},6BP is a downstream gluconeogenesis enzyme which inhibits glycolysis and tumor growth, partly by non-enzymatic mechanisms. The final step of gluconeogenesis is mediated by G-6P, which hydrolyses G-6P to glucose and Pi. In tumor-bearing animals, the activity of gluconeogenic enzymes such as G-6P and F^{-1},6-DP was dramatically reduced. During the development of tumor growth, lactate generation from glucose increases whereas glucose production from pyruvate declines. The lower activity of these enzymes in tumor-bearing animals might be due to the increased lactate production of neoplastic tissues, since it has been proven that tumors need a significant amount of lactate for glycolysis and protein synthesis.[38] In our study, the levels of gluconeogenetic enzymes were significantly lower in DMBA induced cancer bearing rats. Conversely in DG and DG@CS-NP treated rats the situation is reversed. In this context, DG@CS-NP is quite impactful.

TCA cycle is another crucial pathway for oxidative phosphorylation in cells, and it assures that they meet their bioenergetic, biosynthetic, and redox balancing demands. Despite prevalent notion that cancer cells sidestep the TCA cycle in favor of aerobic glycolysis, recent research reveals that certain cancer cells, particularly those with uncontrolled oncogene and tumor suppressor expression, rely significantly on the TCA cycle for energy generation and macromolecule synthesis. The Krebs cycle enzymes catalyses the oxidation of a multitude of substrates in the mitochondria, culminating in reducing equivalent. SDH is a constituent of the inner mitochondrial membrane and is coupled to the ETC directly. Two ATP molecules are produced when succinate is oxidized to form FADH2 molecules, which immediately transmit electrons to ubiquinone. MDH is a NAD-dependent oxidoreductase that catalyses a key step in the Krebs cycle, which is vital for cellular metabolism and energy generation. The activity of these enzymes was reported to be diminished when cancer was evident.[39] Our observations reveal that administering DMBA suppresses TCA cycle enzyme status. On the other hand, the enzymatic status of DG and DG@CS-NP treated rats was restored to near normal levels. Significantly, DG@CS-NP medicated rats showed improved Krebs cycle enzymatic status on compared with DG treated rats. Mammary cancer bearing rats had enzymatic fluctuation of TCA cycle enzymes and carbohydrate metabolizing enzymes. An earlier study found that the mammary cancer bearing experimental animals showed enzymatic alterations in the levels of TCA cycle enzymes, carbohydrate metabolizing enzymes. In DG treated animals, these biochemical modulations returned to near normal levels. As a result, the author states that DG has anticarcinogenic activity against N-methyl-N-nitrosourea induced breast cancer. These findings lend a strong support for our observation of DG's therapeutic impact on carbohydrate metabolism.[31]

Therefore, the levels of glycolytic and pentose phosphate pathway enzyme increased dramatically in rats with mammary carcinoma. It also provokes a reduction in gluconeogenic and mitochondrial enzymes. Concluding, as an intent of precise toxic-free cancer therapeutic interventions, this simple, cost-effective and scalable encapsulated system of DG nanoparticle evidently enhances the specificity of the drug candidate (DG) and the regulated dosage release through ionic gelation method propel it towards effectual targeted therapy. However, the prolonged release resulted from the hydrophobic interaction of polymer-DG within the nanoparticle along with the discharge of DG from the polymeric matrix throughout degradation. This delayed the diffusion of DG from the nanoparticle and allowed for prolonged periods of sustained release for an effective cancer therapy. Evidently, when compared to bare DG treated rats, nano DG significantly reduced the rates of glycolytic enzymes, pentose phosphate pathway enzymes, gluconeogenic enzymes, and mitochondrial enzymes. As a consequence, its chemotherapeutic mechanism of action (Figure 14) on metabolic rewiring has been revealed in experimentally induced rat mammary oncogenesis.

Conclusion

Mammary cancer cells exhibit a high degree of aerobic glycolysis activity, and they profit immensely from this metabolism. As a consequence, anticancer medications might

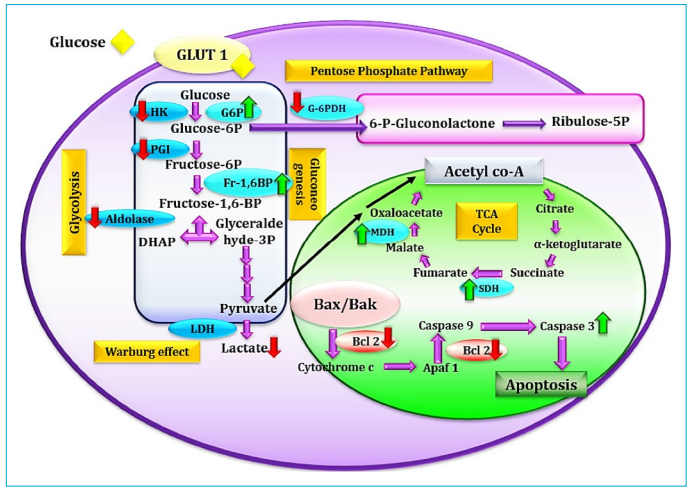

Figure 14. Mechanistic targets of nano diosgenin on carbohydrate metabolizing enzymes.

well be optimally designed using the characteristics and processes of aerobic glycolysis, as well as the link between aerobic glycolysis and cancer growth. Thereby, we were successful in the confirmation of nano DG's anti tumorigenic ability in metabolic rewiring via standardizing the status of various biochemical enzymes in an animal model of DMBA induced mammary oncogenesis. This discovery uncovers a breakthrough therapeutic potential of nano DG against breast cancer and paves the way for future research into leveraging its clinically effective regulation of metabolic cravings in cancerous cells.

Disclosures

Ethics Committee Approval: This study protocol was validated by the IAEC, governed by the Committee for the Purpose of Control and Supervision of Experiments on Animals (CPCSEA), New Delhi, India. (Proposal No. 1241, dated April 23, 2019).

Peer-review: Externally peer-reviewed.

Conflict of Interest: None declared.

Acknowledgments: The authors are thankful to Dr. R. Siranjeevi, Research Associate, SRM University for characterization studies. The authors acknowledge the research resources and assistance provided by Annamalai university's Department of Biochemistry and Biotechnology. Regarding animal maintenance, the authors would like to acknowledge Central animal house, Rajah Muthiah Medical College, and Hospital, Annamalai university.

Conflicts of Interest: The authors confirm that this article content has no conflict of interest.

Authorship Contributions: Concept – M.V.; Design – M.V., M.S.; Supervision – M.S.; Materials –M.V., K.D.; Data collection &/or processing – M.V., K.D.; Analysis and/or interpretation – M.V., K.D., M.S.; Literature search – K.D.; Writing – M.V.; Critical review – M.V., K.D., M.S.

References

1. Manobharathi V, Kalaiyarasi D, Mirunalini S. A concise critique on breast cancer: a historical and scientific perspective. Res J Biotech 2021;16:220–30.
2. Granados-Soler JL, Taher L, Beck J, Bornemann-Kolatzki K, Brenig B, Nerschbach V, et al. Transcription profiling of feline mammary carcinomas and derived cell lines reveals biomarkers and drug targets associated with metabolic and cell cycle –pathways. Sci Rep 2022;12:17025.
3. Wang L, Zhang S, Wang X. The metabolic mechanisms of breast cancer metastasis. Front Oncol 2021;10:2942.
4. Gandhi N, Das GM. Metabolic reprogramming in breast cancer and its therapeutic implications. Cells 2019;8:89.
5. Fan Y, Wang J, Xu Y, Wang Y, Song T, Liang X, et al. Anti-Warburg effect by targeting HRD1-PFKP pathway may inhibit breast cancer progression. Cell Commun Signal 2021;19:18.
6. Ruiz-Iglesias A, Mañes S. The importance of mitochondrial pyruvate carrier in cancer cell metabolism and tumorigenesis. Cancers 2021;13:1488.
7. Hassan MS, Ansari J, Spooner D, Hussain SA. Chemotherapy for BC. Oncol Rep 2010;24:1121–31.
8. Perumal SS, Shanthi P, Sachdanandam P. Energy-modulating vitamins–a new combinatorial therapy prevents cancer cachexia in rat mammary carcinoma. Brit J Nutr 2005;93:901–9.
9. Xu XH, Li T, Fong CM, Chen X, Chen XJ, Wang YT, et al. Saponins from Chinese medicines as anticancer agents. Mol 2016;21:1326.
10. Mirunalini S, Shahira R. Novel effect of diosgenin–a plant derived steroid. A review. Pharmacologyonline 2011;1:726–36.
11. Singh M, Hamid AA, Maurya AK, Prakash O, Khan F, Kumar A, et al. Synthesis of diosgenin analogues as potential anti-inflammatory agents. J Steroid Biochem Mol Biol 2014;143:323–33.
12. Manobharathi V, Mirunalini S. Pharmacological characteristics of a phyto steroidal food saponin: Diosgenin. Afr J Bio S 2020;2:77–87.
13. Jesus M, Martins AP, Gallardo E, Silvestre S. Diosgenin: recent highlights on pharmacology and analytical methodology. J Anal Methods Chem 2016;2016:4156293.
14. Arulmozhi V, Pandian K, Mirunalini S. Ellagic acid encapsulated chitosan nanoparticles for drug delivery system in human oral cancer cell line (KB). Colloids Surf B Biointerfaces 2013;110:313–20.
15. Dudhani AR, Kosaraju SL. Bioadhesive chitosan nanoparticles: Preparation and characterization. Carbohydr Polym 2010;81:243–51.
16. Mohammadi G, Zangeneh MM, Zangeneh A, Haghighi ZM. Chemical characterization and anti-breast cancer effects of silver nanoparticles using Phoenix dactylifera seed ethanolic extract on 7, 12-Dimethylbenz [a] anthracene-induced mammary gland carcinogenesis in Sprague Dawley male rats. Appl Organomet Chem 2020;34:e5136.
17. Isabella S, Mirunalini S. Protective effect of 3, 3'-Diindolylmethane encapsulated chitosan nanoparticles prop up with lipid metabolism and biotransformation enzymes against possible mammary cancer. J App Pharm Sci 2017;7:194–201.
18. Jagadeesan J, Nandakumar N, Rengarajan T, Balasubramanian MP. Diosgenin, a steroidal saponin, exhibits anticancer activity by attenuating lipid peroxidation via enhancing antioxidant defense system during NMU-induced breast carcinoma. J Env Pathol Toxicol Oncol 2012;31:121–9.
19. Kumar BP, Puvvada N, Rajput S, Sarkar S, Das SK, Emdad L, et al. Sequential release of drugs from hollow manganese ferrite nanocarriers for breast cancer therapy. J Mat Chem B 2015;3:90–101.
20. Brandstrup N, Kirk JE, Bruni C. The hexokinase and phosphoglucoisomerase activities of aortic and pulmonary artery tissue in individuals of various ages. J Gerontol 1957;12:166–71.
21. King J. The phosphohydrolases acid and alkaline phospha-

tases. In: King J, editor. Practical and clinical enzymology. London: D. Van Nostrand Co. Ltd.; 1965. p. 121–38.
22. Gracy RW, Tilley BE. Phosphoglucose isomerase of human erythrocytes and cardiac tissue. Methods Enzymol 1975;41:392–400.
23. Ells HA, Kirkman Hn. A colorimetric method for assay of erythrocytic glucose-6-phosphate dehydrogenase. Proc Soc Exp Biol Med 1961;106:607–9.
24. Gancedo J M, Gancedo C. Fructose-1-6-bisphosphatase, phosphofructokinase and glucose-6-phosphate dehydrogenase. Proc Soc Exp Biol Med 1971;106:607–9.
25. Slater EC, Borner WD Jr. The effect of fluoride on the succinic oxidase system. Biochem J 1952;52:185–96.
26. Mehler AH, Kornberg A. The enzymatic mechanism of oxidation-reductions between malate or isocitrate and pyruvate. J Biol Chem 1948;174:961–77.
27. Pal SL, Jana U, Manna PK, Mohanta GP, Manavalan R. Nanoparticle: An overview of preparation and characterization. J Appl Pharm Sci 2011;1:228–34.
28. Jang M, Kim SS, Lee J. Cancer cell metabolism: implications for therapeutic targets. Exp Mol Med 2013;45:e45.
29. Lue HW, Podolak J, Kolahi K, Cheng L, Rao S, Garg D, et al. Metabolic reprogramming ensures cancer cell survival despite oncogenic signaling blockade. Genes Dev 2017;31:2067–84.
30. Siddiqui FA, Prakasam G, Chattopadhyay S, Rehman AU, Padder RA, Ansari MA, et al. Curcumin decreases Warburg effect in cancer cells by down-regulating pyruvate kinase M2 via mTOR-HIF1α inhibition. Sci Rep 2018;8:8323.
31. Vengaimaran M, Dhamodharan K, Sankaran M. Diosgenin nanoparticles competes plain diosgenin on reviving biochemical and histopathological alterations in DMBA induced rat mammary carcinoma via modulating the AhR-Nrf-2 signaling cascades. J Pharm Res Int 2021;33:141–57.
32. Hahm ER, Lee J, Kim SH, Sehrawat A, Arlotti JA, Shiva SS, et al. Metabolic alterations in mammary cancer prevention by withaferin A in a clinically relevant mouse model. J Natl Cancer Inst 2013;105:1111–22.
33. Jagadeesan AJ, Langeswaran K, Kumar SG, Revathy R, Balasubramanian MP. Chemopreventive potential of diosgenin on modulating glycoproteins, TCA cycle enzymes, carbohydrate metabolising enzymes and biotransformation enzymes against N-methyl-N-nitrosourea induced mammary carcinogenesis. Int J Pharm Pharm Sci 2013;5:575–82.
34. Lincet H, Icard P. How do glycolytic enzymes favour cancer cell proliferation by nonmetabolic functions? Oncogene 2015;34:3751–9.
35. Narayanasamy K, Ragavan B. Therapeutic effects of Zanthoxylum tetraspermum WA stem bark on carbohydrate metabolizing enzymes in mammary carcinoma mice. World J Pharm Pharm Sci 2014;3:1092–113.
36. Valle-Mendiola A, Soto-Cruz I. Energy metabolism in cancer: The roles of STAT3 and STAT5 in the regulation of metabolism-related genes. Cancers (Basel) 2020;12:124.
37. Dore MP, Davoli A, Longo N, Marras G, Pes GM. Glucose-6-phosphate dehydrogenase deficiency and risk of colorectal cancer in Northern Sardinia: A retrospective observational study. Medicine (Baltimore) 2016;95:e5254.
38. Grasmann G, Smolle E, Olschewski H, Leithner K. Gluconeogenesis in cancer cells–Repurposing of a starvation-induced metabolic pathway. Biochim Biophys Acta Rev Cancer 2019;1872:24–36.
39. Anderson NM, Mucka P, Kern JG, Feng H. The emerging role and targetability of the TCA cycle in cancer metabolism. Prot Cell 2018;9:216–37.